Cytometry 13:595–602 (1992)

Methods for Topographical Analysis of Intra-Nuclear BrdUrd-Tagged Fluorescence[1]

Yves Usson and Catherine Humbert

Equipe de Reconnaissance des Formes et Microscopie Quantitative, Laboratoire TIM3, USR 00690B C.N.R.S., Université Joseph Fourier, 38041 Grenoble Cedex, France

Received for publication July 19, 1991; accepted December 9, 1991

The observation of BrdUrd staining in the nuclei of cells from exponentially growing populations reveals different typical replicating patterns. We propose a methodological approach to order and characterize BrdUrd intranuclear distributions. First, visual ordering of the patterns is assessed using a spectral analysis coupled to a k-nearest neighbors clustering technique. Subsequently, nine topographical features are introduced to characterize the spatial distribution of BrdUrd-tagged fluorescence in the nuclei of proliferating cells. These topographical features are based on a structural approach. The localization of fluorescence spots is expressed in terms of the normalized distance from the nuclear border and its standard deviation. These topographical features are simple to calculate and easy to relate to visual experience.

Key terms: Topographical features, spectral analysis, BrdUrd patterns

This paper is the first of a pair of articles dealing with BrdUrd texture featuring. In the present paper we address methodological aspects of the analysis of texture. The second paper (9) is dedicated to the study of the sequence of BrdUrd patterns during the S phase of MRC-5 cells cultured in vitro.

Some authors have suggested that eukaryotic DNA replication occurs as a non random process in a reproducible temporal order. Inter-nuclei heterogeneity of the replication site distribution has been observed after the replicated DNA was labelled with BrdUrd (21). These authors qualitatively described the main characteristic of intra-nuclear DNA replication distribution during the S phase. However, this approach remains subjective and there is a real need for quantification. To order these patterns objectively we used a Fourier spectral analysis followed by multifactorial data analysis methods. Subsequently we propose a set of new topographical features with which the spatial distribution of BrdUrd can be expressed quickly and in a comprehensible way. Texture analysis methods have been used in cytometry to investigate the chromatin distribution in cell nuclei (1,4,14,22). Our topographical features are based on a structural approach similar to that introduced by Young et al. to describe the heterogeneity, granularity, and margination of chromatin (22).

MATERIALS AND METHODS

Biological Material

All information concerning the culture of MRC-5 cells, BrdUrd incorporation and indirect immunofluorescence staining of BrdUrd can be found in the second paper of this pair (9).

Image Acquisition

The fluorescence images of 66 BrdUrd-labelled nuclei were photographed using an Axiophot Zeiss (Oberkochen, GDR) photomicroscope with a 485±20 BP exciter filter, a 515–565 BP barrier filter and a ×40 (n.a. 0.75) dry PLAN NEOFLUAR objective (spatial resolution 0.42 μm). Digital images were obtained by digitization of the photographic negatives using a CCD video camera (Tokina CP3000, Tokyo, Japan) connected to a SAMBA cytological image analyzer (Alcatel-TITN-Answare, Grenoble, France). The digitization of photographic negatives insured a good signal to noise ratio and crisp images.

Spectral Texture Analysis and Pattern Ranking

Visual pattern ranking. The BrdUrd images were ordered subjectively. In the first step, a raw order of the

[1]This work was supported by grants from "Pôle Rhône-Alpes Génie Biologique et Médical" and by grant number 6106 from ARC (Association pour la Recherche contre le Cancer).

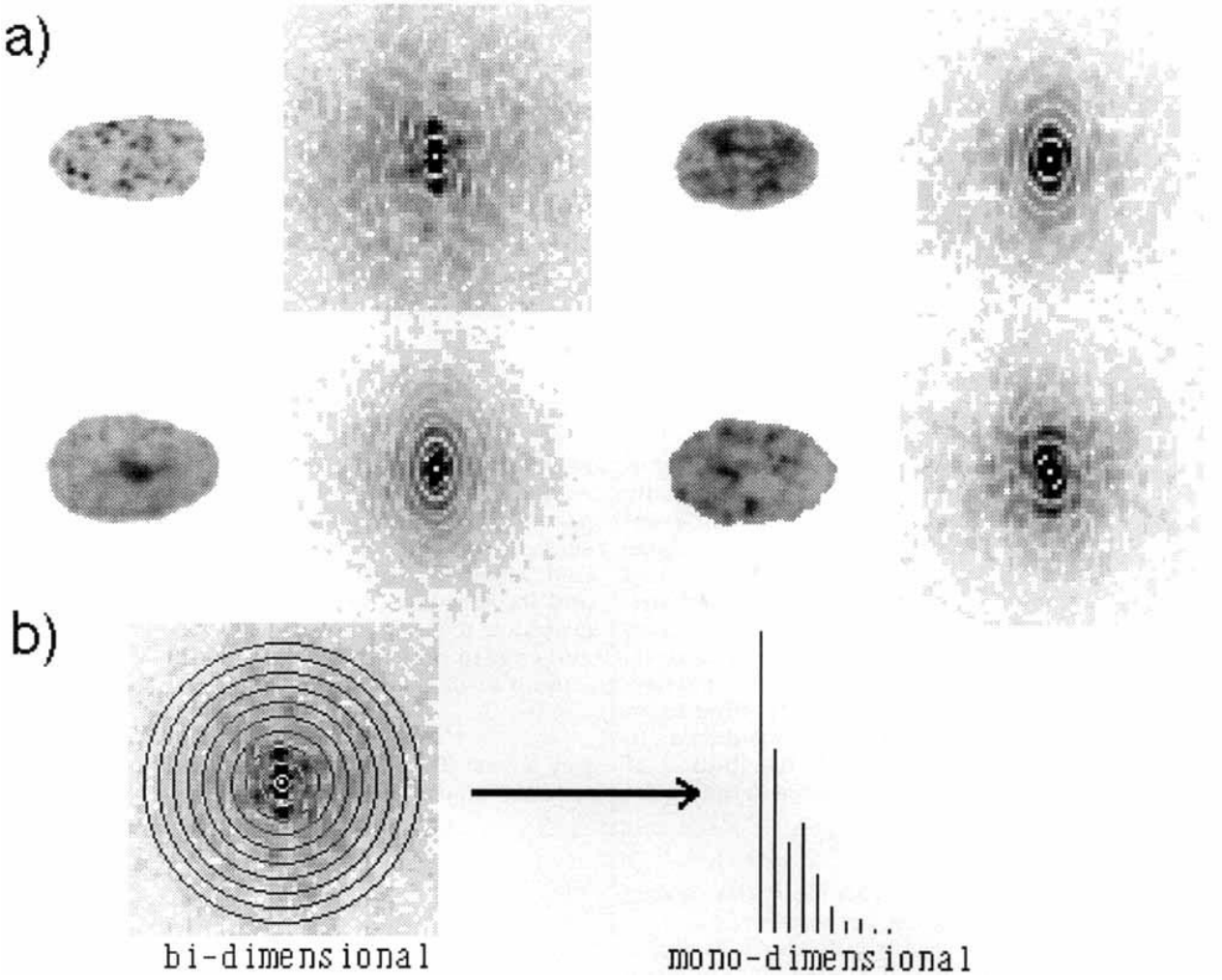

FIG. 1. Fourier spectral analysis. **a)** Example of the bi-dimensional power spectra obtained for four BrdUrd-labelled nuclei. The nuclear images and the power spectra are represented in negative contrast for visual convenience. High intensities of fluorescence and high energy harmonics appear in dark while low fluorescence intensities and low energy harmonics appear in light grey. **b)** Conversion of a bi-dimensional power spectrum into a mono-dimensional one. The magnitude of the harmonics of same rank are averaged along concentric circles centered on the constant component of the power spectrum (white central spot).

patterns was established on the basis of the previously described typical intranuclear DNA replication distribution (21). The second step consisted in refining the first ordering by means of a step by step analysis of pattern similarities.

Fourier analysis. The Fourier spectral analysis was performed on digital images of the nuclei. The size of each image was 128 × 128 square-shaped pixels, with a density of 0.34 μm per pixel. In order to avoid unwanted influence of spatial information, the nucleus was centered in the image and its major axis oriented in parallel with the horizontal axis of the frame prior to digitization. The images were apodized and normalized prior to the Fourier analysis. The apodization consisted in calculating the product of the nuclear image with a two-dimensional cosine function with the same period as the width of the image. This minimized the contribution of pixels on the edge of the image. The second prepocessing was intensity normalization: the average intensity of the image was subtracted from each pixel intensity and the result divided by the standard deviation of intensities in the image. Therefore, all the image power spectra were directly comparable. The Fourier analysis was performed using a two-dimensional Fast Fourier Transform (FFT) programme based on the classical algorithm by Cooley and Tukey (2) (Fig. 1a). Because directional information was not relevant to our study, the two-dimensional power spectrum was transformed into a uni-dimensional one. This was obtained by averaging the magnitude of the harmonics along growing concentric circles originating from the continuous component of the power spectrum (Fig. 1b).

The final result is a spectral signature of each nucleus image based on a spectrum of 64 harmonics.

Cluster analysis. Each power spectrum may be considered to be a vector with 62 components (the continuous component and the first harmonic were discarded because they were identical in all the spectra as a result of intensity normalization). Then, multivariate data analysis tools were used to compare and order the power spectra.

Principal component analysis. Prior to clustering, the power spectra were submitted to Principal Component Analysis (PCA). This method offered the main advantage of reducing a multifactorial space to a small number of factors which summarize most of the information contained in the original space (10,11). First, PCA made it possible to eliminate redundancies and non significant harmonics. Second, it provided a normalized space, well adapted to a clustering algorithm based on Euclidian distances.

K-*Nearest neighbors clustering.* To obtain an objective ranking of BrdUrd textures, the spectral signatures of the nuclei images were analyzed by a k-nearest neighbors (k-NN) clustering algorithm (3,12), where k is the number of neighbors. The principle of k-NN clustering is the following: in a first step the Euclidian distances separating all pairs of spectral signatures in the PCA space were calculated. Then for each nuclear spectral signature we determined the k-nearest spectral signatures, that is, those with the smallest Euclidian distances. Then a graph of the k-NN was made. It consisted in joining each nucleus to its spectral k-nearest neighbors using a distance filter. Only those neighbors among the k-nearest whose distance was smaller than a preset threshold were qualified. In the present study, the number of neighbors (k) was set to 5 and the distance threshold was set to ten percent of the maximum scattering of the projections of the spectral signatures on the first factorial axis of the PCA space.

Pattern ranking was derived from the graph of the k-NN using an algorithm of search for the shortest path in a weighted graph (17). This method consisted in finding the path with the property that the sum of the weights is minimized, with a constraint that prohibits passing twice over the same point. In our k-NN graph the weights were the distances between direct neighbors.

Topographical Pattern Featuring

Nuclear mask segmentation. The segmentation of nuclear masks was achieved in two steps. The first step consisted in a simple level thresholding of the image intensity histogram. This raw thresholding resulted in a satisfactory segmentation for most of the nuclei. However, for nuclei with only a few fluorescent spots a second interactive step was necessary. Thus, the user could redefine or correct the nuclear mask using the interactive graphic tools of the image analysis system.

Intra-nuclear segmentation. The fluorescence intensity histogram of each BrdUrd labelled nucleus was divided in three relative classes: high, medium, and low intensity. The segmentation of these three classes was obtained using a specialized algorithm for automatic grey level classification based on the moving means clustering algorithm (19,20). This segmentation algorithm offered the advantage of being invariant to changes in the image acquisition process. Thus, the result of the three class segmentation was independent of the absolute fluorescence intensity. At the end of the process the nuclear mask was divided in subregions corresponding to the three fluorescence classes (Fig. 2).

Distance encoding. The topographical information inside a nuclear mask was expressed using the shortest distance of a pixel from the border of the nuclear mask. A distance map was created by a classical algorithm of generation of distance curves in a binary mask using the "city block" distance metric (13,16).

Topographical featuring

Features. The principle of calculation of the topographical features is illustrated with the example of nuclear image in Figure 3. For each fluorescence class a histogram of distances from the edge was built using the intersection of the mask of this fluorescence class with the distance map. From this histogram it was possible to compute three variables: the percentage of projection area (A%) of a fluorescence class with reference to the total nuclear projection area, the mean distance from the edge (MD), and the standard deviation of the distances from the edge (SD). The first variable (A%) expresses the relative importance of a fluorescence class, the second variable (MD) gives the average location of the subregions, and the third variable (SD) expressed the heterogeneity of the locations. In order to make the MD and SD variables comparable from one nucleus to another it was necessary that the variables not be influenced by the shape and size of the nuclei. This was made possible by a shape and size normalization.

Shape normalization. One of the drawbacks of using a statistic based on a "distance from the edge" encoding was that in a closed shape such as a nucleus, the pixels close to the edge are more numerous than those far away. This appeared as a decreasing frequency gradient from the edge to the center of a nucleus. Furthermore, the envelope of this gradient is correlated to the shape of a nucleus. Consequently, for a fluorescence class the average distance value obtained directly from the distance histogram would be systematically biased towards the small distances regardless of the position of the sub-regions. For example, if a nucleus had only one high fluorescence spot located midway from the edge to the center of the nucleus, the average value would be significantly smaller than expected. To compensate for this gradient, the frequencies of the distance histograms of each fluorescence class were weighted by the corresponding frequencies of the distance histogram of the total nuclear mask.

Size normalization. For each nucleus, size normal-

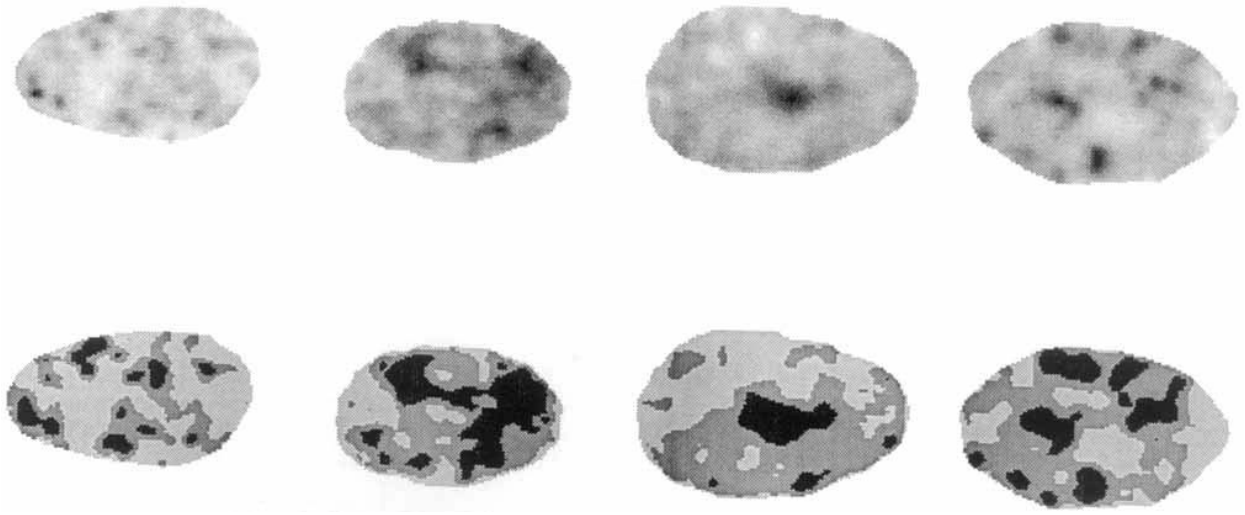

FIG. 2. Intra-nuclear segmentation of the fluorescence histogram. Top line, nuclear images; bottom line, three class segmentation masks. The nuclear images are represented in negative contrast for visual convenience. High intensities of fluorescence appear in dark while low fluorescence intensities appear as light grey. The masks are rendered in black for the high fluorescence class, dark grey for the medium fluorescence class, and light grey for the low fluorescence class. The examination of the segmentation of four examples of nuclei shows very different spatial distributions of the three fluorescence classes.

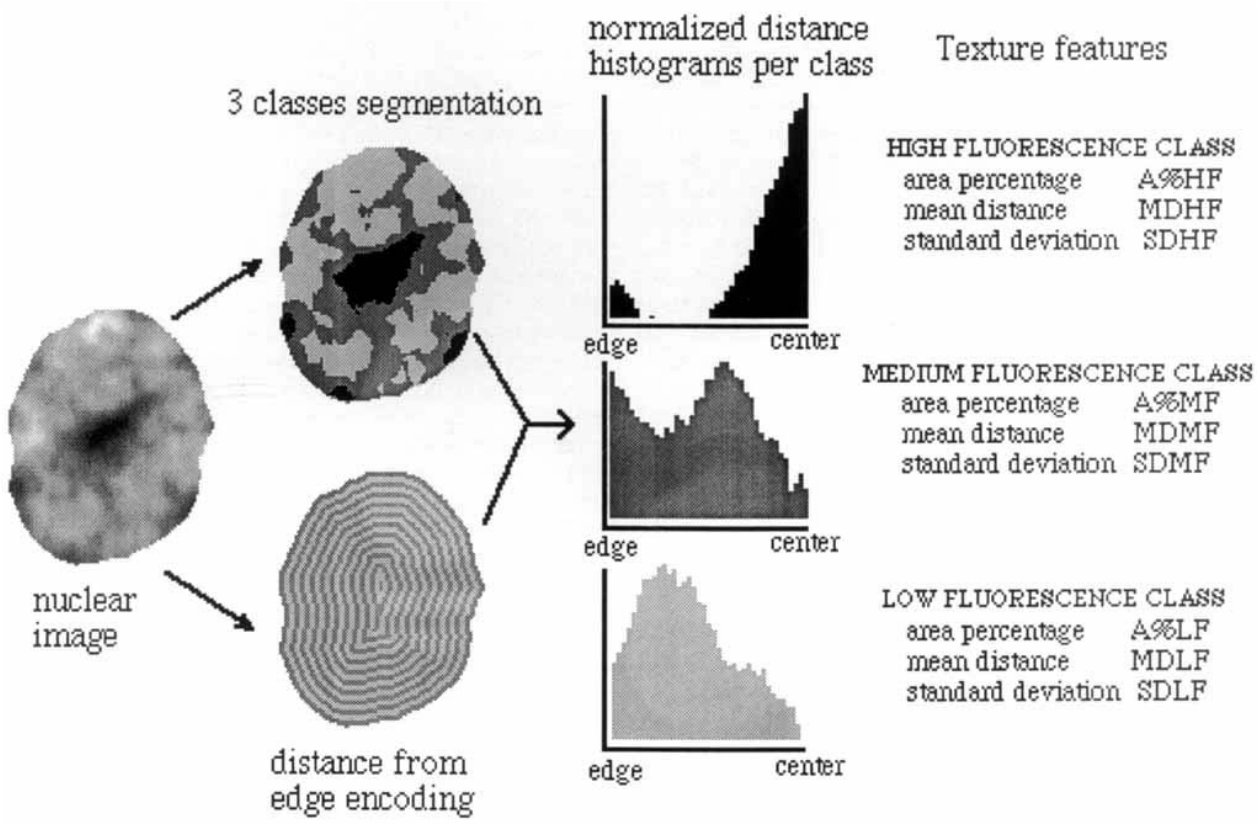

FIG. 3. Topographical texture featuring. The nuclear image is represented in negative contrast for visual convenience. High intensities of fluorescence appear in dark while low fluorescence intensities appear in white. The fluorescence image (left side) of the nucleus is segmented in three classes of fluorescence (high, medium, and low intensity). A distance map is built from the total nuclear mask (distance from the edge encoding); the distances here are symbolized by alternating dark and clear rings. For each fluorescence class, a normalized distance histogram is calculated (see Materials and Methods). From this histogram, three features are calculated: A%, the percentage of projection area with reference to the total nucleus; MD, mean distance from the edge; SD, standard deviation of distances; HF, high fluorescence class; MF, medium fluorescence class; LF, low fluorescence class.

ization consisted in calculating relative distances. These were obtained by dividing the actual distance values by the maximum distance from the edge obtained for that nucleus. Thus, the MD and SD could be expressed as percentages of the maximum distance from the edge (0% on the edge, 100% in the center of the nucleus) and compared directly from one nucleus to another.

When all these normalizations were applied, the final formulas for MD and SD were

$$MD_F = 100 \frac{\sum_{i=1}^{max} \left(\frac{i}{max} \frac{H_F[i]}{H_{nuc}[i]} \right)}{\sum_{i=1}^{max} \left(\frac{H_F[i]}{H_{nuc}[i]} \right)}$$

and

$$SD_F = 100 \frac{\sum_{i=1}^{max} \left[\left(\frac{i}{max} \frac{H_F[i]}{H_{nuc}[i]} \right) - MD_F \right]^2}{\sum_{i=1}^{max} \left(\frac{H_F[i]}{H_{nuc}[i]} \right)},$$

where F is the fluorescence class under consideration, i is the current distance from the edge (integer value), max is the maximum distance in the nucleus, $H_F[i]$ is the frequency of the ith bin of the distance histogram of class F, and $H_{nuc}[i]$ is the frequency of the ith bin of the distance histogram of the total nuclear mask.

RESULTS

All the analyses were performed on a set of 66 BrdUrd-labelled nuclei taken from an exponentially growing cell population. A detailed presentation of these nuclei and their DNA content is given in the second paper of this pair (9).

Spectral Texture Analysis

Fourier analysis. The bi-dimensional power spectra of four typical BrdUrd-tagged nuclei are illustrated in Figure 1a. A power spectrum should be read from its central point to the edges. The central point corresponds to the constant component and the harmonics of same rank are located on the same circle centered on the constant component. From left to right and top to bottom of Figure 1a: the first nucleus exhibited a few small fluorescent spots scattered over the surface of the nucleus. The associated power spectrum showed many high frequencies, the energy being spread up to harmonic 16. In the second nucleus the spots were more numerous and fused to form large ones. This resulted in a concentration of energy in the low frequencies (up to harmonic 5) of the power spectrum. In the third nucleus, a very large central spot was observed, with a few small spots located close to the perinuclear membrane. The spectral distribution was similar to the previous one but contained higher frequencies. Finally, the fourth nucleus contained a few large spots (larger than in the first nucleus) resulting in the presence of high frequencies in the power spectrum.

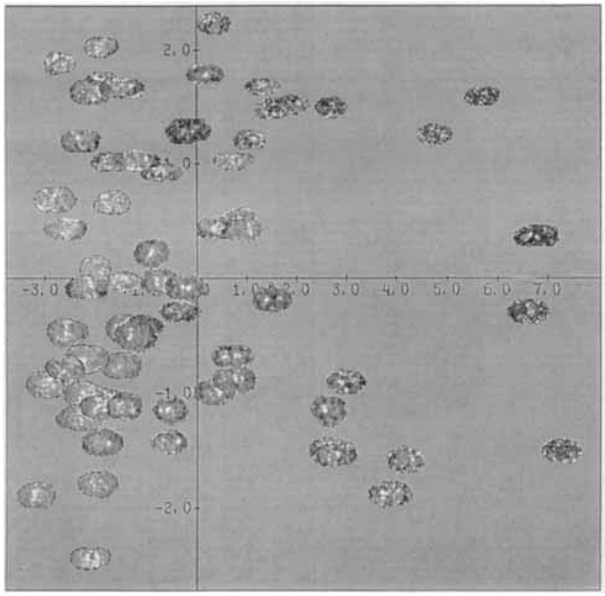

FIG. 4. Factorial plane of the Principal Component Analysis of the spectral signatures. The two factorial axes summarize more than 75% of the total scattering. Reduced images of the nuclei are plotted at the location of projection of their respective spectral signatures. A neutral grey background is used to help visualize small intensity variations in the dark nuclei as well as in the bright nuclei. A black or a white background would squeeze the visual dynamics and therefore make these variations invisible in one or the other category of nuclei.

One can note that for the two-dimensional power spectra the harmonics were not identically distributed along all the directions radiating from the center of the power spectrum. This was due to two reasons: first, the nuclei were elliptical and second, the spots were not evenly distributed in the nuclei. For this reason, in order to reduce the orientation influence, each bi-dimensional power spectrum was converted into mono-dimensional one by averaging the magnitude of the harmonics of the same rank along concentric circles radiating from the center of the power spectrum (Fig. 1b).

Principal component analysis (PCA). In the first step of PCA the correlation matrix of the spectral signatures was calculated. This matrix showed that there was a high correlation (greater than 0.90) between the harmonics of rank higher than 13. Indeed, the magnitude of these harmonics were very low in all the power spectra, and in fact accounted more for the background noise than for significant variations in the images. Therefore, only the harmonics 2 to 13 were taken into account in the following step of the PCA. The analysis of the eigenvalues of the correlation matrix showed that the first six factorial axes summarized 92% of the variance of the original space. Figure 4 shows the projections of the spectral signatures on the first factorial plane. In this figure, the reduced images of the nuclei were plotted at the location of their respective projec-

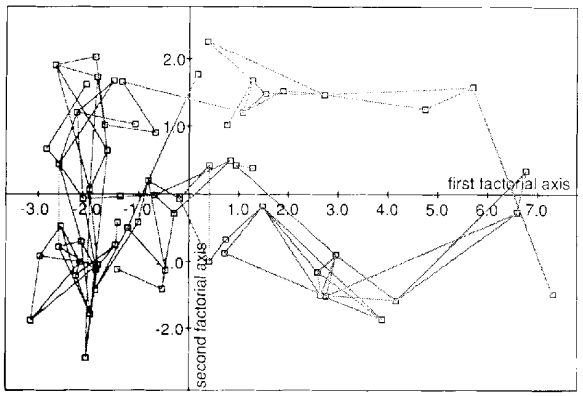

FIG. 5. k-nearest neighbors clustering graph. The graph is plotted on the same factorial plane as in Figure 4. The squares symbolize the projections of the spectral signatures. The grey lines correspond to the link between two projections which satisfy both the k-nearest neighbors rule (with k equal to 5) and the distance criterion (Euclidian distance smaller than 10% of the scattering along the first factorial axis). A ranking can be derived by defining the shortest path between direct neighbors.

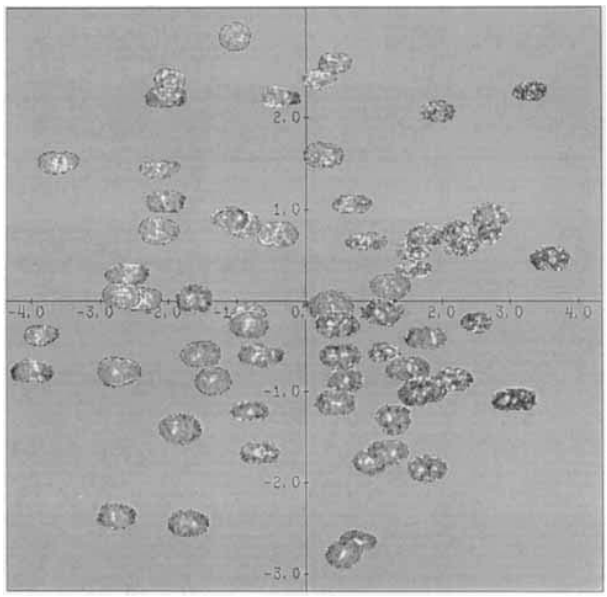

FIG. 6. Factorial plane Principal Component Analysis of the topographical features. The two factorial axes summarize more than 80% of the total scattering information. Reduced images of the nuclei are plotted at the location of their respective projection. A neutral grey background is used to help visualize small intensity variations in the dark nuclei as well as in the bright nuclei. A black or a white background would squeeze the visual dynamic and therefore make these variations invisible in one or the other category of nuclei.

tions. The analysis of the projections of the different harmonics on the factorial axes showed that the harmonics with rank greater than 7 mainly contributed to the first factorial axis. Therefore, it tended to separate nuclei with high frequencies, that is, with small spots, from nuclei poor in high frequencies, that is, with a less heterogeneous texture. Smaller rank harmonics mainly contributed to the second and third axes. These axes tended to separate the nuclei as function of the size and localization of spots.

Pattern Ranking

To obtain an objective ranking of BrdUrd patterns a k-nearest neighbors clustering algorithm was applied to the projections of the spectral signatures on the factorial axes. Figure 5 illustrates the graph of the k-NN obtained with k equal to 5. This graph shows the neighborhood relationships between the nuclei. It can be seen that there is a pathway starting from the right side of factorial plane and running towards the upper left side. Subsequently, it runs from the top to the bottom and eventually ends on the right side of the plane. The left part of the graph looks very confused but most of it can be untangled when the third factorial axis is taken into account. It is a common artefact of PCA projections: two points that look close to each other on a factorial plane may be in fact very distant along another dimension (i.e., third axis). Searching the shortest path in this graph from one end to the other made it possible to establish an objective ranking of the different patterns. This ordering was then compared to the visual ranking. It appeared that these were compatible: most of the nuclei were ranked similarly or some were displaced a maximum of plus or minus 3 ranks. Only four nuclei were found to be in completely different ranks (discrepancy of more than 10 ranks). A Spearman rank correlation test was used to assess the agreement of the spectral signature ranking and the visual ranking. A correlation value of 0.98 was obtained and differed significantly from 0 at a 0.001 threshold. This objective ranking was used as a basis for a fine analysis of the changes of BrdUrd-tagged fluorescence during S phase of the cell cycle (9).

Topographical Pattern Features

The topographical features were measured for each of the 66 nuclei. These measurements were submitted to a PCA. Figure 6 shows the projections of the nuclei on the first factorial plane of the PCA. It appeared that the nuclei were not randomly distributed but were grouped specifically as a function of their fluorescence patterns. The analysis of the projections of the topographical variables on the factorial axes (Table 1) showed that the percentage area of high fluorescence (A%HF), on one hand, and the three variables of the low fluorescence class (A%LF, MDLF, SDLF), on the other, mainly contributed to the first factorial axis. A%HF pointed to the left side of the plane; A%LF, MDLF, and SDLF pointed to the right side. Thus, the nuclei with labelling spread over the whole nuclear area were mainly on the left plane and nuclei with the labelling concentrated in a few spots were mainly on the right plane. The variables MDHF, SDMF, and

Table 1
Principal Component Analysis of the Nine Topographical Variables[a]

	A%HF	MDHF	SDHF	A%MF	MDMF	SDMF	A%LF	MDLF	SDLF
1st axis	−0.83	−0.33	0.19	−0.05	0.46	0.29	0.84	0.90	0.81
2nd axis	0.28	−0.62	−0.59	−0.10	0.38	0.72	−0.14	−0.10	−0.04

[a]Respective contributions of the variables to the two first factorial axes of the PCA. Contributions are dimensionless and a value close to 1 in absolute value corresponds to a maximum contribution A%, percentage of area; MD, mean distance from the edge; SD, standard deviation of the distances; HF, high fluorescence; MF, medium fluorescence; LF, low fluorescence.

SDHF contributed to the second axis. Thus, the second axis separated nuclei with many fluorescent spots distributed all over their surface (upper plane) from nuclei with a large central spot and perinuclear spots (lower plane). The nuclei with many spots had a medium MDHF and high SDMF values expressing an even spatial distribution of fluorescence. The nuclei with a large central spot had high MDHF values expressing the concentration of labelling in the central part; the high SDHF expressed the spatial heterogeneity due to the perinuclear spots. The other variables (A%MF, MDMF) mainly contributed to third and fourth factorial axes.

DISCUSSION

The observation of BrdUrd staining in the nuclei of cells from exponentially growing populations reveals different typical replicating patterns (21). Some authors have attempted to order these patterns as a function of visual similitudes. However, this ordering remains subjective and there is a real need for quantification. Our first goal was to define an objective ranking of these patterns. A robust method to characterize a texture pattern is spectral analysis (15). The clustering algorithm based on Euclidian distances made it possible to analyze the neighborhood relationships of the nuclear spectral signatures and thereafter to establish a hierarchy. It is interesting to note that the k-nearest neighbors clustering method gave an ordering that was not basically different (rank correlation 0.98) from that established visually. There were only a few discrepancies, and after a posteriori examination of these particular cases the new ranking defined by the clustering method was found to be acceptable. In fact, these were cases that could be visually assigned to two possible ranks. In conclusion, the representation of the patterns by their spectral signatures is a powerful method. However, the spectral analysis does not give any clue on the exact location of the labelling spots inside the nuclei and therefore it is not useful for interpretation of replication patterns. As an alternative we proposed a set of variables with which the spatial distribution of BrdUrd-tagged fluorescence could be expressed in a comprehensible way.

Image analysis techniques have been used now for many years in the domain of cytometry (1) and different methods have been developed to quantify textural features in cells (14). For example, texture analysis has proved to be an efficient tool to analyse the condensation of chromatin in the different phases of the cell cycle (6,22) and to investigate the maturation of the erythroblastic cell lineage (5,7). These methods are generally classed in two categories: stochastic methods (4,8) and structural methods (8,22). The stochastic methods are based on the use of statistical matrices such as cooccurrence and gray level run-length matrices (4). From these matrices a set of independant variables are calculated. These variables were found to be very satisfactory for describing the various condensation states of the chromatin during the cell cycle (6,7,18). However, these variables are very difficult to comprehend and to relate to visual experience. The structural methods use a different approach which consists in identifying different physical structures (i.e., dark or bright spots) and calculating the localization of these with reference to a particular point (22). It has the main advantage of providing variables that can be directly interpreted with respect to visual experience. Following the same principles of the structural approach, we developed a set of topographical variables. To translate the "clumpiness" of the labelling in the nucleus we converted the image of the nucleus in a three intensity class image using a principle similar to that used by Young et al. (22). For each of these classes, the localization was expressed as the mean distance from the edge and the associated standard deviation. We chose the edge of the nucleus as a reference instead of the center of gravity because it corresponds to a consistently identifiable biological structure, i.e., the nuclear membrane. Conversely, the center of gravity does not correspond to any identifiable structure, and its location may not necesserally fall inside the limits of the nucleus as it is the case for example in a polynuclear blood cell. Furthermore, if two spots are located at the same distance from the edge of an elliptic nuclei, but one is on the minor axis and the other on the major axis, their distances from the center of gravity are different.

In conclusion, the main advantage of these topographical features is their simplicity. They are independent of the size and the shape of the nucleus, and also are independent of the overall fluorescence intensity. They do not require time consuming calculations (1 s per nucleus). With the recent introduction of confocal laser scanning microscopy in biology there will be a need for three-dimensional texture analysis tools. Our topographical features can be easily adapted to studies of volumic textures.

LITERATURE CITED

1. Brugal G: Image analysis of microscopic preparations. In: Methods and Achievement in Experimental Pathology, Jasmin G and Proscheck L (eds). Karger, Basel, 1984, 11: pp. 1–33.
2. Cooley JW, Tukey JW: An algorithm for the machine calculation of complex Fourier series. Math Comp 19:297–301, 1965.
3. Fukunaga K: Introduction to Statistical Pattern Recognition. Academic Press, New York, 1972.
4. Galloway MM: Texture analysis using gray level run lengths. Computer Graphics Image Processing 4:172–179, 1975.
5. Gauvain C, Seigneurin D, Brugal G: A quantitative analysis of the human bone marrow erythroblastic cell lineage using the SAMBA 200 cell image processor. I. The normal maturation sequence. Analyt Quant Cytol Histol 9:253–262, 1987.
6. Giroud F: Cell nucleus pattern analysis: geometric and densitometric featuring, automatic cell phase identification. Biol Cell 44:177–188, 1982.
7. Giroud F, Gauvain C, Seigneurin D, von Hagen V: Chromatin texture changes related to proliferation and maturation in erythrocytes. Cytometry 9:339–348, 1988.
8. Haralick RM: Statistical and structural approaches to texture. Proceedings of the Fourth International Joint Conference on Pattern Recognition, IAPR (eds), Kyoto, 1978, pp. 45–69.
9. Humbert C, Usson Y: Topographical Analysis of BrdUrd labeled nuclei: Eukaryotic DNA replication is a topographically ordered process. (Submitted).
10. Kendall MG: Multivariate Analysis. Charles Griffin, London, 1975.
11. Manly BFJ: Principal component analysis. In: Multivariate Statistical Methods: A Primer. Chapman and Hall, London, New York, 1986, pp 59–71.
12. Manly BFJ: Cluster analysis. In: Multivariate Statistical Methods: A Primer. Chapman and Hall, London, New York, 1986, pp. 100–113.
13. Montanvert A: Medial Line: graph representation and shape description. In: 8th International Conference on Pattern Recognition, IAPR (eds), Paris, 1986, pp. 430–432.
14. Pressman NJ, Haralick RM, Tyrer HW, Frost JK: Texture analysis for biomedical imagery. In: Biomedical Pattern Recognition and Image Processing, Fu KS and Pavlidis T (eds). Verlag Chemie, Florida Basel, 1979, pp. 153–178.
15. Russ JC: Computer Assisted Microscopy: The Measurement and Analysis of Images. Plenum Press, New York London, 1990.
16. Russ JC, Russ JC: Uses of the euclidian distance map for the measurement of features in the images. J Comp Assist Microsc 1:343–375, 1989.
17. Sedgewick R: Algorithm in C. Addison-Wesley, New York, Workingham, Tokyo, 1990.
18. Usson Y, Saxod R: Schwann cell proflieration in the sciatic nerve of hypothyroid chick embryos studied by autoradiography and image analysis. J Neurocytol 17:639–648, 1988.
19. Usson Y, Torch S, Drouet d'Aubigny G: A method for automatic classification of large and small myelinated fibre populations in peripheral nerves. J Neurosci Methods 20:237–248, 1987.
20. Usson Y, Torch S, Saxod R: Morphometry of human nerve biopsies by means of automated cytometry: Assessment with reference to ultrastructural analysis. Analyt Cell Pathol 3:91–102, 1991.
21. van Dierendonck JH, Keyzer R, van de Velde CJH, Cornelisse CJ: Subdivision of S-phase by analysis of nuclear 5-bromodeoxyuridine staining patterns. Cytometry 10:143–150, 1989.
22. Young IT, Verbeek PW, Mayall BH: Characterization of chromatin distribution in cell nuclei. Cytometry 7:467–474, 1986.